Damping of toroidal ion temperature gradient modes

H. Sugama
National Institute for Fusion Science, Toki 509-5292, Japan

(Received 26 March 1999; accepted 1 June 1999)

The temporal evolution of linear toroidal ion temperature gradient (ITG) modes is studied based on a kinetic integral equation including an initial condition. It is shown how to evaluate the analytic continuation of the integral kernel as a function of a complex-valued frequency, which is useful for investigating the asymptotic damping behavior of the ITG mode. In the presence of the toroidal magnetic drift, the potential perturbation consists of normal modes and a continuum mode, which correspond to contributions from poles and from an integral along a branch cut, respectively, of the Laplace-transformed potential function of the frequency. The normal modes have exponential time dependence while the continuum mode, which has a ballooning structure, shows a power law decay $\propto t^{-2}$, where t is the time variable. Therefore, the continuum mode dominantly describes the long-time asymptotic behavior of the perturbation for the stable system. By performing proper analytic continuation for the dispersion relation, the normal modes' growth rate, real frequency, and eigenfunction are numerically obtained for both stable and unstable cases. © *1999 American Institute of Physics.* [S1070-664X(99)02009-1]

I. INTRODUCTION

So far, many theoretical studies have been done on microinstabilities such as ion temperature gradient (ITG) modes[1] as a cause of anomalous transport in high temperature plasmas. Most linear analyses of these microinstabilities[2–6] have shown the dispersion relation only for the case of positive growth rates, mainly because the anomalous transport is driven by unstable modes and partly because calculation of negative growth rates is sometimes more complicated due to treatment of analytic continuation in the complex-frequency plane. However, since stable modes with negative growth rates play the role of an energy sink for turbulence in order to realize a steady state, they would seem to affect the saturation amplitude of the turbulence and the resultant anomalous transport. For example, gyrofluid simulations[7] produce steady-state turbulence even in the collisionless limit by successfully modeling kinetic stabilizing mechanisms such as Landau damping and finite Larmor radius (FLR) effects. Thus, in order to consider the balance of fluctuation energy, it is useful to obtain the complete dispersion relation including both stable and unstable modes. Also, if we can calculate both positive and negative growth rates, the critical condition for the marginal stability can be determined more accurately by interpolation.

In the case of parallel transit resonance, which occurs between waves and particles moving along field lines, it is well-known how to draw a Landau contour for analytic continuation of the plasma dispersion function.[8] For toroidal systems, the magnetic ∇B-curvature drift modifies wave-particle resonance and therefore complicates how to analytically continue the dispersion function. Under the local approximation, where the inhomogeneity in the direction parallel to the field line is neglected to enable us to specify the parallel wave number $k_\parallel$ as an independent parameter, several studies have been done of the analytic continuation of the dispersion function for the ITG mode driven by these magnetic drifts, in order to evaluate damping rates of stable normal modes.[9–11] An interesting aspect of the toroidal magnetic resonance, which is absent from the parallel transit resonance, is that the analytic continuation for the toroidal mode requires a branch cut to be taken in the lower-half complex-frequency plane. Kuroda *et al.*[11] investigated an initial value problem for the toroidal ITG mode in the local approximation and found that components with complex frequencies along the branch cut yield a continuum mode which shows power-law decay oscillation.

The present work is an extension of that by Kuroda *et al.* to the nonlocal case where the mode structure along the field line remains to be solved for by taking account of the parallel inhomogeneity. Here analytical continuation for the nonlocal problem is properly treated to calculate the growth rate, real frequency, and eigenfunction for stable modes. We will find for the nonlocal case that a branch cut also appears and that a general solution of an initial value problem of the toroidal ITG mode for the nonlocal case consists of normal modes and a continuum mode which shows a different power-law decay from that for the local case.

The rest of this work is organized as follows. In Sec. II, a linear electrostatic ion gyrokinetic equation and its Laplace transform are presented. The ballooning representation is used to treat the nonlocal structure of perturbations in a toroidal system. The temporal behavior of the ballistic response in the presence of the toroidal magnetic drift is elucidated. In Sec. III, an initial value problem for the toroidal ITG mode is formulated as a Laplace-transformed integral equation for the electrostatic potential perturbation. It is shown how to analytically continue the integral equation into the lower-half complex-frequency plane. The temporal evolution of the potential perturbation is written as the sum of the normal modes and the continuum mode, for which the long-time asymptotic behavior is determined. In Sec. IV, following the

prescription for analytic continuation given in Sec. III, the integral equation is numerically solved to obtain the dependencies of the normal modes' growth rate, real frequency, and eigenfunction on η_i (the ratio of the ion temperature gradient to the density gradient), k_θ (the poloidal wave number), $\hat{s}$ (the magnetic shear parameter), and θ_k (the ballooning angle corresponding to the minimum radial wave number) for both stable and unstable cases. Finally, conclusions are given in Sec. V.

II. ION GYROKINETIC EQUATION

In this section, we first consider the Laplace transform of the ion gyrokinetic equation in order to include the initial condition of the perturbation. Using it, the ballistic response of the ions in the presence of toroidal magnetic drifts is described.

A. Laplace transform of the gyrokinetic equation

The ion distribution function in the $(\boldsymbol{x},\boldsymbol{v})$ phase space is divided into the equilibrium and perturbation parts as $f_i = n_0 F_M + \delta f_i$ where n_0 is the equilibrium density, $F_M \equiv \pi^{-3/2} v_{Ti}^{-3} \exp(-v^2/v_{Ti}^2)$ is the Maxwellian distribution function, and $v_{Ti} \equiv (2T_i/m_i)^{1/2}$ is the thermal velocity for the ions with mass m_i, temperature T_i, and electric charge e. In the magnetic field $\boldsymbol{B}$, the perturbation part δf_i with the perpendicular wave number vector $\boldsymbol{k}_\perp$ is written as

$$\delta f_i = -\frac{e\phi}{T_i} n_0 F_M + h e^{-i\boldsymbol{k}_\perp \cdot \boldsymbol{\rho}}, \tag{1}$$

where ϕ represents the electrostatic potential, $\boldsymbol{\rho} \equiv \boldsymbol{b} \times \boldsymbol{v}/\Omega_i$ ($\boldsymbol{b} = \boldsymbol{B}/B$) denotes the ion gyroradius vector, and $\Omega_i \equiv eB/(m_i c)$ is the ion gyrofrequency. Here, the first and second terms in the right-hand side of Eq. (1) represent the adiabatic and nonadiabatic parts, respectively. The velocity vector $\boldsymbol{v}$ is written as $\boldsymbol{v} = v_\parallel \boldsymbol{b} + v_\perp (\boldsymbol{e}_1 \cos\xi + \boldsymbol{e}_2 \sin\xi)$, where ξ is the gyrophase and $(\boldsymbol{e}_1, \boldsymbol{e}_2, \boldsymbol{b})$ are unit vectors which form a right-handed orthogonal system at each point. The ion nonadiabatic distribution function h is independent of the gyrophase and is described in the linear, collisionless, electrostatic case by the gyrokinetic equation[12,13]

$$\left(\frac{\partial}{\partial t} + \frac{v_\parallel}{Rq}\frac{\partial}{\partial \theta} + i\omega_D\right) h = \left(\frac{\partial}{\partial t} + i\omega_{*T}\right) \frac{e\phi}{T_i} \times J_0(k_\perp \rho) n_0 F_M, \tag{2}$$

with

$$\omega_D \equiv \hat{\omega}_D [\cos\theta + \hat{s}(\theta - \theta_k)\sin\theta] v_{Ti}^{-2} \left(\frac{v_\perp^2}{2} + v_\parallel^2\right) \tag{3}$$

and

$$\omega_{*T} = \omega_{*i}\left[1 + \eta_i \left\{\left(\frac{v}{v_{T_i}}\right)^2 - \frac{3}{2}\right\}\right], \tag{4}$$

where J_0 is the Bessel function of order zero, q is the safety factor, $\hat{s} = (r/q)(dq/dr)$ is the magnetic shear parameter, r and R are the minor and major radii, respectively, $\eta_i \equiv d\ln T_i/d\ln n_0$ is the ratio of the ion temperature gradient to the density gradient, $\hat{\omega}_D \equiv 2\epsilon_n \omega_{*i}$ is the characteristic ion ∇B-curvature drift frequency, $\omega_{*i} \equiv -\tau_e^{-1}\omega_{*e}$ is the ion diamagnetic drift frequency, $\epsilon_n \equiv L_n/R$ is the ratio of the equilibrium density gradient scale length $L_n \equiv -(d\ln n_0/dr)^{-1}$ to the major radius R, $\tau_e \equiv T_e/T_i$ is the ratio between the electron and ion temperatures, $\omega_{*e} \equiv ck_\theta T_e/(eBL_n)$ is the electron diamagnetic drift frequency, $k_\theta = nq/r$ is the poloidal wave number, and n is the toroidal mode number. In Eqs. (2) and (3), we have assumed a large-aspect-ratio axisymmetric toroidal system with circular, concentric magnetic surfaces, and used the ballooning representation to regard the poloidal angle θ as a coordinate along the magnetic field line which forms a so-called *covering space* $(-\infty < \theta < \infty)$.[14,15]

Using the Laplace transform

$$h(\omega) = \int_0^\infty dt\ h(t) e^{i\omega t}, \tag{5}$$

Eq. (2) is rewritten as

$$\left[\frac{v_\parallel}{Rq}\frac{\partial}{\partial\theta} - i(\omega - \omega_D)\right] h(\omega) = -i(\omega - \omega_{*T})\frac{e\phi}{T_i} J_0(k_\perp\rho) n_0 F_M + \langle \delta f_i(t=0) e^{i\boldsymbol{k}_\perp\cdot\boldsymbol{\rho}}\rangle, \tag{6}$$

where $\langle\cdots\rangle$ denotes the gyrophase average.

Throughout this work, following Dong *et al.*[2] and Romanelli,[3] the toroidal effect is considered only through the poloidal-angle-dependent magnetic drift given by Eq. (3) which causes the ballooning structure of the ITG mode. The trapped ions and the poloidal-angle dependence of the parallel velocity $v_\parallel$ are neglected here since mainly the passing ions drive the ITG mode.

B. Ballistic response

Here we consider the ballistic response to the initial perturbation in the presence of the toroidal resonance, which is determined by the propagator on the left-hand side of the gyrokinetic equation (2). A similar problem was treated already by Kim *et al.*[10] and Kuroda *et al.*[11] for the case of the local approximation which specifies the parallel wave number $k_\parallel$. They showed that, under the local approximation, the asymptotic temporal dependence of the ballistic response is characterized by $t^{-3/2}\exp(-i\omega_{br}t)$ where $\omega_{br} = -k_\parallel^2 v_{Ti}^2/(4\hat{\omega}_D)$. In the problem considered in this work, the fluctuations' structure along the field line is not generally represented by a sinusoidal wave corresponding to a single parallel wave number, which cannot be a linear eigenfunction due to the toroidicity of the magnetic drift.

Let us consider the case in which $\phi = 0$ in order to neglect the right-hand side of the gyrokinetic equation (2). Then, the solution of Eq. (2) is given by

$$h(\theta,\omega) = \begin{cases} \displaystyle\int_{-\infty}^{\theta} d\theta'(Rq/|v_\parallel|)e^{i\beta(\theta,\theta')}h(\theta',t=0) & \text{for } v_\parallel>0 \\ \displaystyle\int_{\theta}^{\infty} d\theta'(Rq/|v_\parallel|)e^{-i\beta(\theta,\theta')}h(\theta',t=0) & \text{for } v_\parallel<0, \end{cases} \tag{7}$$

with

$$\beta(\theta,\theta') = \int_{\theta'}^{\theta} d\theta''(Rq/|v_\parallel|)[\omega-\omega_D(\theta'')]. \tag{8}$$

Here, as noted before, only the passing ions have been considered in deriving Eq. (7). Then, using Eq. (2), the Laplace transform of the ion density perturbation is written as

$$\begin{aligned}\delta n_i(\omega) &= \int d^3v\ J_0(k_\perp\rho)h(\omega) \\ &= 2\pi\int_0^\infty v_\perp dv_\perp \int_0^\infty dv_\parallel \int_{-\infty}^{\infty} d\theta'(Rq/v_\parallel) \\ &\quad\times e^{i\beta(\theta,\theta')\mathrm{sgn}(\theta-\theta')}h(\theta',t=0).\end{aligned} \tag{9}$$

Here, we assume the initial distribution to have the form

$$h(\theta,t=0) = C_h J_0(k_\perp\rho)F_M\delta n(\theta,t=0), \tag{10}$$

where C_h is a constant. From the condition that $\delta n(t=0) = \int d^3v J_0(k_\perp\rho)h(t=0)$, we have $C_h = 1/\Gamma_0(b_i)$ where $b_i = k_\perp^2\rho_{Ti}^2/2$, $\rho_{Ti}^2 = v_{Ti}^2/\Omega_i^2 = 2c^2m_iT_i/(e^2B^2)$, $\Gamma_0(b_i) = I_0(b_i)\exp(-b_i)$, and I_0 is the modified Bessel function of order zero. The above form of the initial distribution is taken in order to simplify comparison to the case of the initial value problem including self-consistent potential fluctuations considered in the next section. Substituting Eq. (10) into Eq. (9), we obtain

$$\begin{aligned}\delta n(\omega) &= \frac{C_h}{\sqrt{\pi}}\int_0^{+\infty} d\tau e^{i\omega\tau}\int_{-\infty}^{+\infty} dk' \frac{e^{-(k-k')^2/4\lambda}}{\sqrt{a\lambda}(1+a)} \\ &\quad\times\Gamma_0(k_\perp,k_\perp')\,\delta n(k',t=0).\end{aligned} \tag{11}$$

Here, following Dong *et al.*,[2] we have used variables defined by

$$\tau = Rq|\theta-\theta'|/|v_\parallel|, \tag{12}$$

$$\lambda = \frac{\tau^2}{\tau_e a}\left(\frac{\hat{s}}{q}\epsilon_n\right)^2\omega_{*e}^2, \tag{13}$$

$$a = 1 + i\frac{\tau}{(\theta-\theta')}\int_{\theta'}^{\theta} d\theta''\omega_D(\theta''), \tag{14}$$

$$k = \hat{s}k_\theta(\theta-\theta_k), \quad k' = \hat{s}k_\theta(\theta'-\theta_k), \tag{15}$$

$$\Gamma_0(k_\perp,k_\perp') = I_0\left(\frac{k_\perp k_\perp'}{\tau_e(1+a)}\right)\exp\left(-\frac{k_\perp^2+k_\perp'^2}{2\tau_e(1+a)}\right), \tag{16}$$

$$k_\perp^2 = k_\theta^2+k^2, \quad k_\perp'^2 = k_\theta^2+k'^2, \tag{17}$$

where the wave numbers k_θ, $k_\perp$, and k are normalized by ρ_s^{-1} with $\rho_s \equiv \sqrt{2T_e/m_i}/\Omega_i$. In the ballooning representation, the radial wave number k is directly related to the poloidal angle θ as the covering-space coordinate by Eq. (15), which implies that the radial mode structure is given by the Fourier transform of the poloidal mode structure. The integral parameter τ in Eqs. (11) and (14) has the opposite sign to that in Ref. 2.

The form of Eq. (11) directly shows its inverse Laplace transform for the density perturbation as a function of time to be given by

$$\begin{aligned}\delta n(t) &= \frac{C_h}{\sqrt{\pi}}\int_{-\infty}^{+\infty} dk' \frac{e^{-(k-k')^2/4\lambda}}{\sqrt{a\lambda}(1+a)} \\ &\quad\times\Gamma_0(k_\perp,k_\perp')\,\delta n(k',t=0).\end{aligned} \tag{18}$$

Here, λ and a are regarded as functions of t which are obtained by replacing τ with t in Eqs. (13) and (14), respectively. By using Eq. (18) with a specified initial density profile $\delta n(k,t=0)$, we can completely determine the spatio-temporal behavior of the density perturbation $\delta n(k,t)$. If we neglect the magnetic shear ($\hat{s}=0$) and the θ (or k) dependence of ω_D in Eq. (3) and assume that the initial perturbation has the sinusoidal form $\propto\exp(ik_\parallel Rq\theta)$ with a parallel wave number $k_\parallel$,

$$\begin{aligned}\delta n(t) &= \frac{2C_h}{\sqrt{a}(1+a)}\Gamma_0\left(\frac{k_\theta^2}{\tau_e(1+a)}\right) \\ &\quad\times\exp\left(-\frac{k_\parallel^2v_{Ti}^2t^2}{4a}\right)\delta n(t=0),\end{aligned} \tag{19}$$

which is the same result as given by the local analysis in Refs. 10 and 11. Here, $a = 1+i\hat{\omega}_D t$. Then, we find from Eq. (19) that, in the presence of the ∇B-curvature drift, the ballistic mode shows the power-law decay oscillation $\propto t^{-3/2}\exp(-i\omega_{br}t)$ $[\omega_{br}\equiv -k_\parallel^2v_{Ti}^2/(4\hat{\omega}_D)]$ in the asymptotic limit.

However, the sinusoidal form assumed in deriving Eq. (19) does not satisfy the boundary conditions $\lim_{\theta\to\pm\infty}\delta n(\theta)=0$ which is required by the ballooning representation. Thus, we consider a more appropriate initial profile for a toroidal system, which is given in the Gaussian form

$$\delta n(t=0) = \delta n(\theta=0,\ t=0)\exp[-(Rq\theta/L)^2]. \tag{20}$$

Then, substituting Eq. (20) into Eq. (18) gives

$$\begin{aligned}\delta n(t) &= \delta n(\theta=0,\ t=0)\frac{2C_h}{1+a}((v_{Ti}t/L)^2+a)^{-1/2} \\ &\quad\times\Gamma_0\left(\frac{k_\theta^2}{\tau_e(1+a)}\right)\exp\left(-\frac{a(Rq\theta/L)^2}{(v_{Ti}t/L)^2+a}\right).\end{aligned} \tag{21}$$

We find from Eq. (21) with $a = 1+i\hat{\omega}_D t$ that the asymptotic behavior of the ballistic mode is governed by the power-law decay

$$\delta n(t=0) = \delta n(\theta=0,\ t=0)\frac{2C_hL}{i\hat{\omega}_D v_{Ti}}t^{-2} \quad \text{for } t\to\infty. \tag{22}$$

Comparing this expression with the asymptotic form of Eq. (19), the oscillation part $\exp(-i\omega_{br}t)$ is replaced by $t^{-1/2}$. This is considered to be valid for general perturbations satisfying the ballooning boundary conditions $\lim_{\theta\to\pm\infty}\delta n(\theta)=0$. Since such perturbations are expressed as a continuous spectrum consisting of sinusoidal waves $\propto\exp(ik_\parallel Rq\theta)$, the initial density perturbation is written as $\delta n(t=0)=\int dk_\parallel F(k_\parallel)\exp(ik_\parallel Rq\theta)$, where $F(k_\parallel)$ is the amplitude of the Fourier component with the parallel wave number $k_\parallel$ [$F(k_\parallel)$ has a Gaussian form for the case of Eqs. (20)–(22)]. Recalling that the time evolution of the sinusoidal waves in Eq. (19) shows the power-law decay oscillation $\propto t^{-3/2}\exp(-i\omega_{br}t)$ with $\omega_{br}=-k_\parallel^2 v_{Ti}^2/(4\hat{\omega}_D)$, the asymptotic behavior of the density perturbation $\delta n(t)$ is obtained as

$$\delta n(t)\propto\int dk_\parallel F(k_\parallel)t^{-3/2}\exp(-i\omega_{br}t)\propto t^{-2}\quad\text{for}\quad t\to\infty. \tag{23}$$

III. TIME EVOLUTION OF THE TOROIDAL ITG MODE

The ballistic mode behavior considered in the previous section does not take account of a self-consistent electrostatic field. Here, in addition to the ion gyrokinetic equation, we use an adiabatic electron response and the quasineutrality condition to self-consistently solve an initial value problem for the toroidal ITG mode.

A. Formulation of the toroidal ITG mode as an initial value problem

In the presence of the electrostatic perturbation ϕ, the Laplace-transformed gyrokinetic equation (6) is solved under the same approximation as in the previous subsection to give the ion density perturbation δn_i, and we assume the electron density perturbation δn_e to satisfy the Boltzmann relation $\delta n_e/n_0=e\phi/T_e$. Then, using the quasineutrality condition $\delta n_e=\delta n_i$, we obtain an integral equation

$$(1+\tau_e)\hat{\phi}(k)-\int_{-\infty}^{+\infty}\frac{dk'}{\sqrt{2\pi}}K(k,k')\hat{\phi}(k')=I(k), \tag{24}$$

where $\hat{\phi}=e\phi/T_e$ is the normalized electrostatic potential and the integral kernel K is defined by

$$\begin{aligned}K(k,k')=&-i\int_0^{+\infty}\omega_{*e}\,d\tau\frac{\sqrt{2}e^{i\omega\tau}}{\sqrt{a\lambda}(1+a)}e^{-(k-k')^2/4\lambda}\\&\times\Gamma_0(k_\perp,k_\perp')\left[\frac{\omega}{\omega_{*e}}\tau_e+1-\frac{3}{2}\eta_i+\frac{\eta_i(k-k')^2}{4a\lambda}\right.\\&\left.+\frac{2\eta_i}{(1+a)}\left(1-\frac{k_\perp^2+k_\perp'^2}{2(1+a)\tau_e}+\frac{k_\perp k_\perp'}{(1+a)\tau_e}\,\frac{I_1}{I_0}\right)\right].\end{aligned} \tag{25}$$

Here, the initial condition

$$\langle\delta f_i(\theta,t=0)e^{i\mathbf{k}_\perp\cdot\boldsymbol{\rho}}\rangle=C_f J_0(k_\perp\rho)F_M\delta n(\theta,t=0) \tag{26}$$

with $C_f=-\tau_e+(1+\tau_e)/\Gamma_0(b_i)$, is used to write the right-hand side of Eq. (24) as

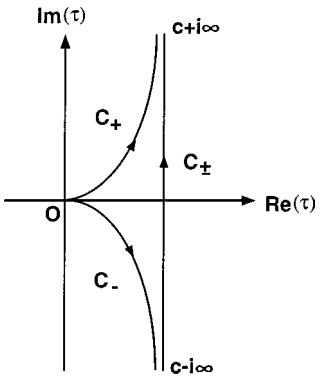

FIG. 1. Curves C_+, C_-, and $C_\pm$ in the complex τ-plane. The curve C_+ (C_-) is used as the τ-integral path in Eq. (25) to obtain the analytical continuation of the kernel K_+ (K_-) into the lower right-hand (left-hand) complex ω-plane defined by $\omega_i<0$ and $\omega_r>0$ ($\omega_r<0$). The curve $C_\pm$ gives the τ-integral path to obtain the jump $\Delta K\equiv K_+-K_-$ on the branch cut C_{br} (see Fig. 2).

$$\begin{aligned}I(k)=&\frac{C_f}{\sqrt{\pi}}\int_0^{+\infty}d\tau e^{i\omega\tau}\int_{-\infty}^{+\infty}dk'\frac{e^{-(k-k')^2/4\lambda}}{\sqrt{a\lambda}(1+a)}\\&\times\Gamma_0(k_\perp,k_\perp')\,\delta n(k',t=0)\end{aligned} \tag{27}$$

which has the same right-hand side as Eq. (11).

Equation (24) is in the form of a Fredholm integral equation of the second kind[16] and its solution can be formally written in terms of the resolvent kernel $M(k,k')$ [see Eq. (62) in Ref. 16 for the resolvent kernel] as

$$\begin{aligned}\hat{\phi}(k)&=(1+\tau_e)^{-1}\left[I(k)+\int_{-\infty}^{+\infty}dk'M(k,k')I(k')\right]\\&\equiv(\mathcal{L}I)(k),\end{aligned} \tag{28}$$

where $\mathcal{L}$ denotes the inversion operator.

Then, the time evolution of the electrostatic potential is given by the inverse Laplace transform of $\phi(k,\omega)$ in Eq. (28) as

$$\hat{\phi}(k,t)=\int_L\frac{d\omega}{2\pi}\,\hat{\phi}(k,\omega)e^{-i\omega t}, \tag{29}$$

where L is a contour which lies above all of the singular points of $\phi(\omega)$ in the complex ω-plane. In order to elucidate the asymptotic behavior of the perturbation in the limit $t\to\infty$, we need to know how to choose a contour L and how to analytically continue the functions of ω in Eqs. (25) and (27), which is considered next.

B. Analytic continuation in the complex-frequency plane

We see that the τ-integral in Eq. (25) does not converge for $\omega_i\equiv\gamma\equiv\mathrm{Im}(\omega)<0$. Here, we find how to evaluate the analytic continuation of the kernel K into the region $\omega_i<0$. We regard the integral valuable τ as complex-valued and we change the integral path from the positive real τ-axis to those in the complex τ-plane as shown in Fig. 1. In Fig. 1, the curves C_+ and C_- both start from the origin $\tau=0$ and are tangential to the real τ-axis at $\tau=0$. The curve C_+ ap-

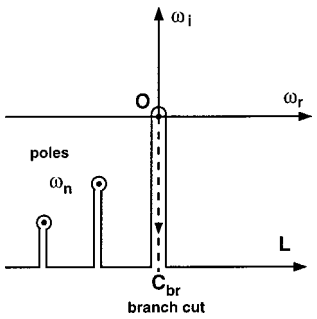

FIG. 2. The integration contour L in the complex ω-plane for evaluating the inverse Laplace transform Eq. (29). The dominant contributions to the integral are made by poles ω_n and a branch cut C_{br}.

proaches $\tau = c + i\infty$ (c: a positive real constant), satisfying $\mathrm{Re}(\tau) > 0$ and $\mathrm{Im}(\tau) > 0$, while the curve C_- approaches $\tau = c - i\infty$, satisfying $\mathrm{Re}(\tau) > 0$ and $\mathrm{Im}(\tau) < 0$. Let us define a new kernel K_+ by Eq. (25), using the curve C_+ for the path of the τ-integral. We should note that, when continuously changing the original path along the positive real τ-axis to the curve C_+, any singular points of the integrand in the complex τ-plane are crossed. We also note that, if we consider the integral along a curve connecting the end points of these two paths $\tau = c + i\infty$ and $\tau = +\infty$, it contributes nothing. Thus, we find that, as functions of ω, K and K_+ have the same value on the quarter plane defined by the $\omega_r \equiv \mathrm{Re}(\omega) > 0$ and $\omega_i > 0$. By noting that the new kernel K_+ is a well-defined analytic function of ω in the right-hand half-plane $\omega_r > 0$, we conclude that K_+ gives the analytic continuation of K into the lower right-hand quarter-plane defined by the $\omega_r > 0$ and $\omega_i < 0$. In a similar way, we can use the curve C_- to define a kernel K_- which gives the analytic continuation of K into the lower left-hand quarter-plane defined by the $\omega_r < 0$ and $\omega_i < 0$.

Now, we observe that K_+ and K_- defined in this way approach different values as ω approaches a branch cut C_{br} which is defined as a straight line from $\omega = 0$ to $\omega = -i\infty$ (see Fig. 2). The jump on the branch cut is written as

$$K_+ - K_- = \Delta K, \tag{30}$$

where ΔK is given by Eq. (25) with the τ-integral performed along the path $C_\pm$ connecting $\tau = c + i\infty$ and $\tau = c - i\infty$ (see Fig. 1). In a similar way to K_+, K_-, and ΔK, we can define I_+, I_-, and ΔI by using C_+, C_-, and $C_\pm$ as the τ-integral paths in Eq. (27), respectively.

The complex-valued eigenvalues ω_n ($n = 1,2,\cdots$) are defined as the ω's, which allow nontrivial solutions $\phi(\omega)$ of the homogeneous version of the integral equation (24) obtained by putting the right-hand side to zero. It is well known that the real and imaginary parts of these eigenvalues describe the real frequencies and growth rates of so-called normal modes, respectively. The same homogeneous integral equation was numerically solved by Dong *et al.* for the cases of positive growth rates.[2] As shown later by numerical examples, we can calculate these eigenvalues not only for positive growth rates but also for negative ones with proper analytic continuation using K_+ and K_-. Then, we observe that, as a function of ω, the inversion operator $\mathcal{L}(\omega)$ in Eq. (28) has these eigenvalues as singular points or poles and that C_{br} can also be regarded as a branch cut for the analytic continuation of $\mathcal{L}(\omega)$ and $I(\omega)$.

C. Normal modes and continuum mode

Now, we take the integration contour L for evaluating the inverse Laplace transform in Eq. (29) as shown in Fig. 2. Then, for $t > 0$, $\phi(t)$ is written as the sum of the contributions from the poles and the branch cut

$$\hat{\phi}(t) = \hat{\phi}_p(t) + \hat{\phi}_{br}(t). \tag{31}$$

Here, the pole contribution, which are from the normal modes, is given by

$$\hat{\phi}_p(k,t) = -i \sum_n e^{-i\omega_n t}\, \mathrm{Res}[(\mathcal{L}I)(k,\omega_n)], \tag{32}$$

where $\mathrm{Res}[(\mathcal{L}I)(k,\omega_n)]$ denotes the residue of $(\mathcal{L}I)(k,\omega)$ at a pole $\omega = \omega_n$. The eigenvalues (or complex-valued normal-mode frequencies) ω_n in Eq. (32) are numerically calculated in the next section including the case of negative growth rates.

The contribution from the branch cut, which is called a continuum mode, is written as

$$\hat{\phi}_{br}(k,t) = \int_{C_{br}} \frac{d\omega}{2\pi} e^{-i\omega t} [(\mathcal{L}_+ I_+)(k,\omega) - (\mathcal{L}_- I_-)(k,\omega)], \tag{33}$$

where the subscripts $+$ $(-)$ for $\mathcal{L}$ and I represent their values on the branch cut defined by the limit of the analytical continuation in the right-hand (left-hand) lower-half plane for $\omega_r \to +0$ ($\omega_r \to -0$). The asymptotic behavior of $\hat{\phi}_{br}(t)$ for $t \to +\infty$ is dominantly determined by the behavior of the integrand of Eq. (33) in the limit $\omega_i \to -0$. For $\omega_i \to -0$, the jumps $\Delta\mathcal{L} \equiv \mathcal{L}_+ - \mathcal{L}_-$ and $\Delta I \equiv I_+ - I_-$ become so small that we have

$$\begin{aligned}[(\mathcal{L}_+ I_+)(k,\omega = i\omega_i) - (\mathcal{L}_- I_-)(k,\omega = i\omega_i)] \\ \simeq [\mathcal{L}(\omega = 0)\Delta I](k,\omega = i\omega_i) \\ + [\Delta\mathcal{L}(\omega = i\omega_i) I](k,\omega = 0) \quad \text{for} \quad \omega_i \to -0.\end{aligned} \tag{34}$$

Here, $\Delta\mathcal{L}(\omega = i\omega_i)$ is written as

$$\Delta\mathcal{L}(\omega = i\omega_i) \simeq \mathcal{L}(\omega = 0)\Delta\mathcal{K}(\omega = i\omega_i)\mathcal{L}(\omega = 0), \tag{35}$$

where the operator $\Delta\mathcal{K}(\omega = i\omega_i)$ is defined for an arbitrary function $g(k)$ by

$$
\begin{aligned}
&[\Delta\mathcal{K}(\omega=i\omega_i)g](k)\\
&\quad\equiv\int_{-\infty}^{+\infty}\frac{dk'}{\sqrt{2\pi}}\Delta K(k,k',\omega=i\omega_i)g(k')\\
&\quad\simeq 2\sqrt{\pi}|\omega_i|\left(1-\frac{3}{2}\eta_i\right)\left|\frac{\sqrt{\tau_e}q}{\hat{s}\epsilon_n\omega_{*e}}\right|\\
&\qquad\times\int_{-\infty}^{+\infty}dk'\left(\frac{i}{(\theta-\theta')}\int_{\theta'}^{\theta}d\theta''\omega_D(\theta'')\right)^{-1}g(k')\\
&\qquad\text{for }\ \omega_i\to-0.
\end{aligned}
\tag{36}
$$

We also have

$$
\begin{aligned}
\Delta I(k,\omega=i\omega_i)\simeq 2\sqrt{\pi}|\omega_i|iC_f&\left|\frac{\sqrt{\tau_e}q}{\hat{s}\epsilon_n\omega_{*e}}\right|\\
&\times\int_{-\infty}^{+\infty}dk'\left(\frac{i}{(\theta-\theta')}\int_{\theta'}^{\theta}d\theta''\omega_D(\theta'')\right)^{-1}\\
&\times\frac{\delta n(k',t=0)}{n_0}\qquad\text{for }\ \omega_i\to-0.
\end{aligned}
\tag{37}
$$

From Eqs. (33)–(37), we obtain

$$
\begin{aligned}
\hat{\phi}_{br}(k,t)\simeq\frac{t^{-2}}{\sqrt{\pi}}&\left|\frac{\sqrt{\tau_e}q}{\hat{s}\epsilon_n\omega_{*e}}\right|\mathcal{L}(\omega=0)\\
&\times\int_{-\infty}^{+\infty}dk'\left(\frac{i}{(\theta-\theta')}\int_{\theta'}^{\theta}d\theta''\omega_D(\theta'')\right)^{-1}\\
&\times\left[C_f\frac{\delta n(k',t=0)}{n_0}-i\left(1-\frac{3}{2}\eta_i\right)\right.\\
&\left.\times[\mathcal{L}(\omega=0)I](k',\omega=0)\right]\qquad\text{for }\ t\to+\infty.
\end{aligned}
\tag{38}
$$

Noting that $\delta n_i/n_0=\delta n_e/n_0=\hat{\phi}$ and comparing Eq. (38) with Eq. (22), we see that, for the initial value problem for the toroidal ITG mode, the potential and density perturbations derived from the branch cut integration show the same form of asymptotic behavior $\propto t^{-2}$ as the density perturbation for the ballistic mode without interaction with the potential. [When $\mathcal{L}=1$, $\Delta L=0$, $\hat{\omega}_D=$const, and the initial density perturbation profile in Eq. (20) are used, the ballistic mode result in Eq. (22) is reproduced from Eq. (38).] This power-law decay is difficult to describe using the gyro-fluid model, since it approximates the dispersion function by a rational function of ω which never requires any branch cut for its analytic continuation.[17]

From Eqs. (31), (32), and (38), we arrive at the conclusion, which is similar to the result of the local analysis,[11] that the long-time asymptotic behavior of the potential and density perturbations for the toroidal ITG mode are determined by the normal mode with the largest positive growth rate for the unstable case, while it is dominated by the continuum mode for the stable case in which all normal modes decay faster than the continuum mode, although the power law $\propto t^{-2}$ of the decay for the continuum mode is different from $t^{-3/2}e^{-i\omega_{br}t}$ in the local case.

It should be remarked here that we can also make different branch cuts in the ω-plane from the one considered here. Different branch cuts make differences in the definitions of $\phi_p(t)$ and $\phi_{br}(t)$ because of changes in the complex-frequency regions where the analytic continuation of $K(\omega)$, $I(\omega)$, and $\mathcal{L}(\omega)$ are defined. However, the total perturbation $\phi(t)=\phi_p(t)+\phi_{br}(t)$ and its asymptotic behavior given by Eq. (38) for the stable case are independent of the way the branch cut is made. In our choice of the branch cut along the negative imaginary axis of ω, the integrand in Eq. (33) quickly decays along the integral path, so that the continuum mode part of the total perturbation is likely to be smaller than that obtained by some other choice of the branch cut. Therefore, for the stable case, the normal mode part defined in our case is likely to decay slower than in other cases.

Kuroda, *et al.*[11] showed a numerical example of temporal evolution of the ITG mode for the local stable case, in which the continuum mode is perceived only after the normal modes, which are dominant in the early stage, are well damped. So if large collisional effects are included, they may prevent the continuum mode from being clearly seen.

IV. NUMERICAL SOLUTION FOR STABLE AND UNSTABLE NORMAL MODES

In this section, the homogeneous version of the integral equation (24) is numerically solved to obtain real frequencies, growth rates, and eigenfunctions of the normal modes. In order to treat the case of negative growth rates, we follow the prescription shown in the previous section to evaluate the analytic continuation of the integral kernel as a function of ω. For the numerical results shown here, we actually calculate the kernel by using the integral paths in the complex τ-plane defined by

$$
\tau=\begin{cases}(1+i|\omega|s)s & \text{for }\ \omega_r>0\\ (1-i|\omega|s)s & \text{for }\ \omega_r<0,\end{cases}
\tag{39}
$$

where s $(0\leqslant s<\infty)$ is a real parameter. These integral paths work for the analytic continuation as well as C_+ and C_-, described in the previous section.

Figures 3(a) and (b) show the numerically obtained normalized growth rate $\gamma k_\theta\rho_s/\omega_{*e}$ and real frequency $\omega_r k_\theta\rho_s/\omega_{*e}$ of the toroidal ITG mode, respectively, as a function of the normalized poloidal wave number $k_\theta\rho_s$ for $\tau_e=1$, $\epsilon_n=0.2$, $\eta_i=2$, $\hat{s}=1$, $\theta_k=0$, and $q=1,\ 2$. Here the normalization unit frequency $\omega_{*e}/(k_\theta\rho_s)=\sqrt{T_e/2m_e}/L_n$ is independent of k_θ. We see that the growth rate and real frequency are smoothly continued into the stable regions where the growth rate is negative, which shows that our procedure for analytic continuation works properly. Stable regions are found for both small and large poloidal wave numbers, which was also observed in the calculations using the local approximation. For all curves shown in Fig. 3(b), the real frequency is negative, which corresponds to the direction of the ion diamagnetic rotation. The eigenfunctions

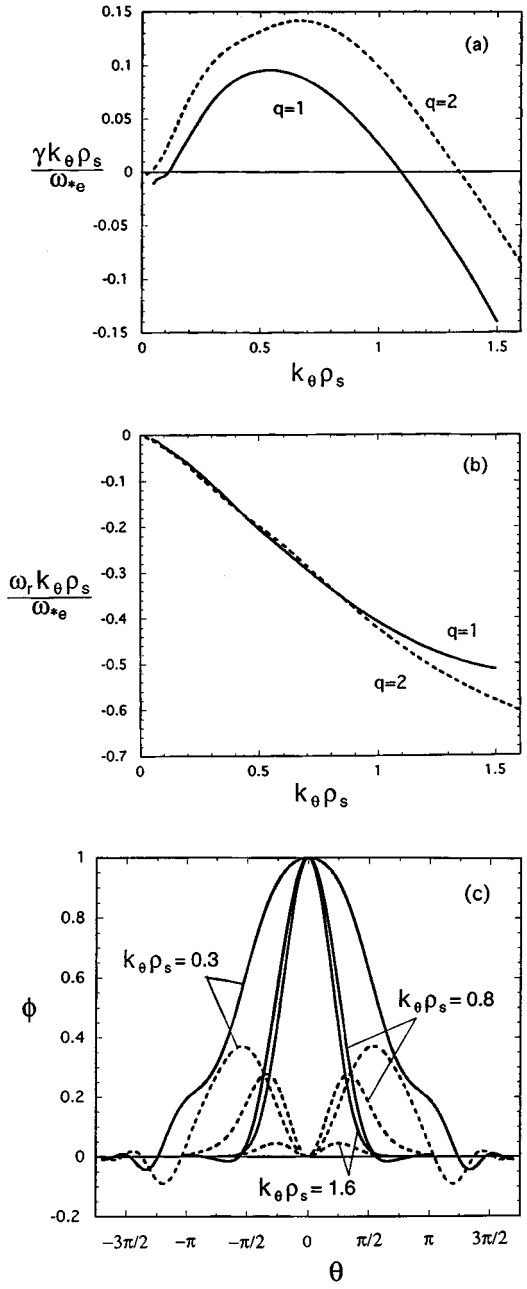

FIG. 3. (a) Normalized growth rate $\gamma k_\theta \rho_s / \omega_{*e}$ and (b) real frequency $\omega_r k_\theta \rho_s / \omega_{*e}$ as a function of $k_\theta \rho_s$ for $\tau_e = 1$, $\epsilon_n = 0.2$, $\eta_i = 2$, $\hat{s} = 1$, $\theta_k = 0$, and $q = 1$, 2. (c) Eigenfunctions $\phi(\theta)$ for $k_\theta \rho_s = 0.3$, 0.8, 1.6 and $q = 2$ with other parameters being the same as in (a) and (b). The real and imaginary parts of the eigenfunction are shown by the solid and dotted lines, respectively.

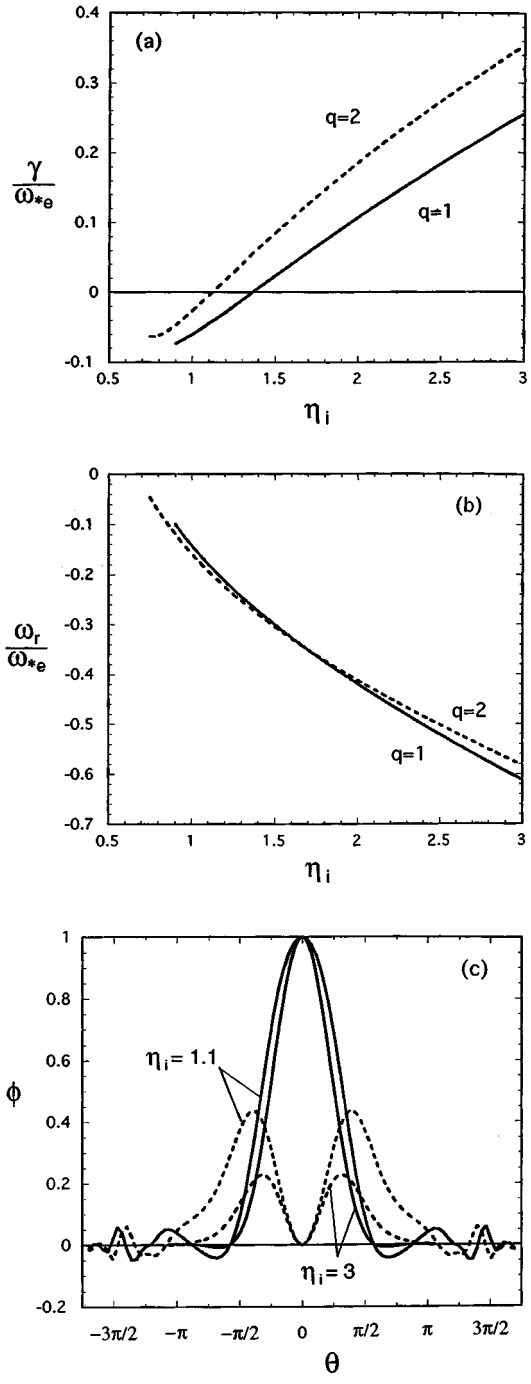

FIG. 4. (a) Normalized growth rate γ / ω_{*e} and (b) real frequency ω_r / ω_{*e} as a function of η_i for $\tau_e = 1$, $\epsilon_n = 0.2$, $k_\theta \rho_s = 0.75$, $\hat{s} = 1$, $\theta_k = 0$, and $q = 1$, 2. (c) Eigenfunctions $\phi(\theta)$ for $\eta_i = 1.1$, 3 and $q = 2$ with other parameters being the same as in (a) and (b). The real and imaginary parts of the eigenfunction are shown by the solid and dotted lines, respectively.

$\phi(\theta)$ for $k_\theta \rho_s = 0.3$, 0.8, 1.6 and $q = 2$ are shown in Fig. 3(c), where the other parameters are the same as in Figs. 3(a) and (b). Here, the real and imaginary parts of the eigenfunction are shown by the solid and dotted lines, respectively. For smaller poloidal wave numbers, the eigenfunction becomes wider and more oscillatory along the field line.

Figures 4(a) and (b) show the normalized growth rate γ / ω_{*e} and real frequency ω_r / ω_{*e} of the toroidal ITG mode, respectively, as a function of η_i for $\tau_e = 1$, $\epsilon_n = 0.2$, $k_\theta \rho_s = 0.75$, $\hat{s} = 1$, $\theta_k = 0$, and $q = 1$, 2. Since we are able to calculate both positive and negative growth rates, we can clearly identify the critical values of η_i where the growth rate vanishes. The eigenfunctions $\phi(\theta)$ for $\eta_i = 1.1$, 3 and $q = 2$ are shown in Fig. 4(c), where the other parameters are the same as in Figs. 4(a) and (b). For $\eta_i = 1.1$, the growth rate is negative (but close to marginal stability) and the eigenfunction is slightly wider and more oscillatory than the unstable eigenfunction for $\eta_i = 3$.

The effects of negative magnetic shear on ITG modes have been theoretically investigated by several authors[18,19] in

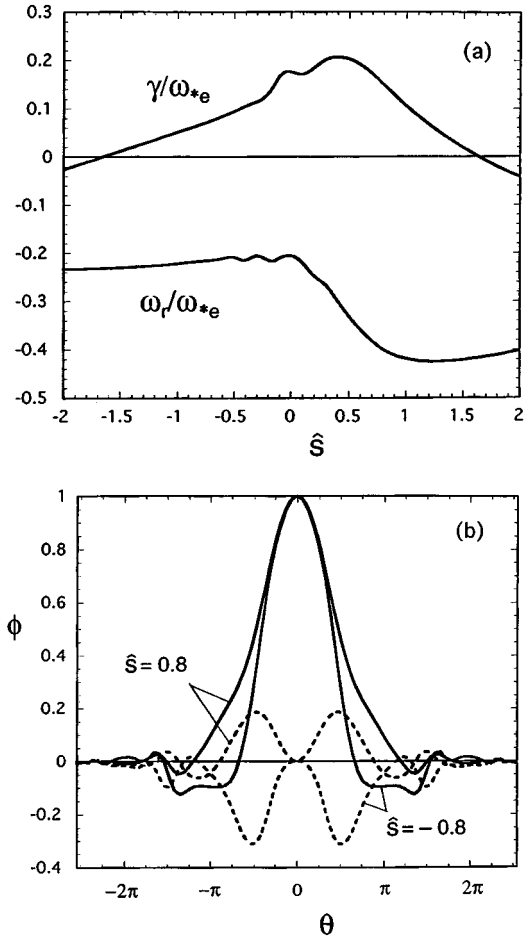

FIG. 5. (a) Normalized growth rate γ/ω_{*e} and real frequency ω_r/ω_{*e} as a function of $\hat{s}$ for $\tau_e=1$, $\epsilon_n=0.2$, $\eta_i=2$, $k_\theta\rho_s=0.75$, $\theta_k=0$, and $q=1$. (b) Eigenfunctions $\phi(\theta)$ for $\hat{s}=\pm 0.8$ with other parameters being the same as in (a). The real and imaginary parts of the eigenfunction are shown by the solid and dotted lines, respectively.

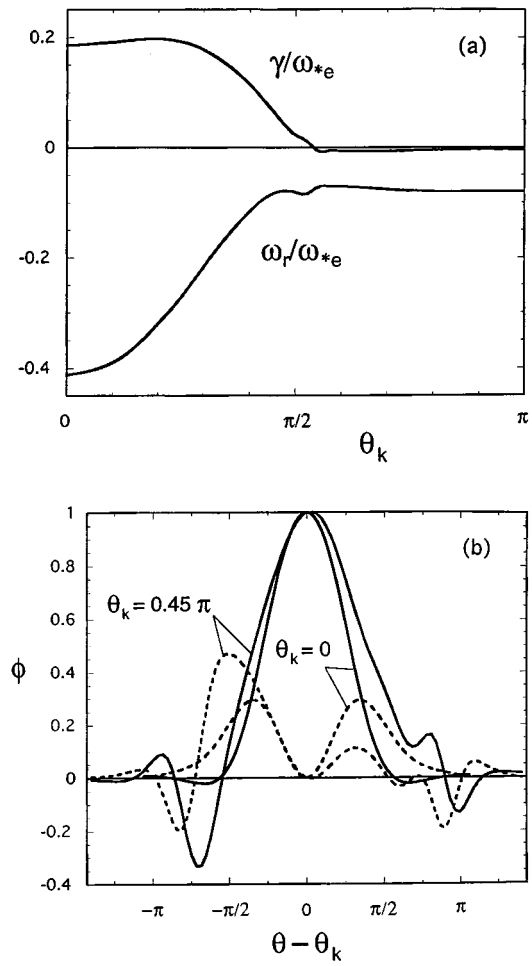

FIG. 6. (a) Normalized growth rate γ/ω_{*e} and real frequency ω_r/ω_{*e} as a function of θ_k for $\tau_e=1$, $\epsilon_n=0.2$, $\eta_i=2$, $\hat{s}=1$, $k_\theta\rho_s=0.75$, and $q=2$. (b) Eigenfunctions $\phi(\theta)$ for $\theta_k=0$, 0.45π with other parameters being the same as in (a). The real and imaginary parts of the eigenfunction are shown by the solid and dotted lines, respectively.

relation to improvement of core plasma confinement observed in large tokamaks.[20–22] However, the results in these works only showed the dependence of positive growth rates on the magnetic shear. In Fig. 5(a), the normalized growth rate γ/ω_{*e} and real frequency ω_r/ω_{*e} as a function of $\hat{s}$ for $\tau_e=1$, $\epsilon_n=0.2$, $\eta_i=2$, $k_\theta\rho_s=0.75$, $\theta_k=0$, and $q=1$. In this case, the growth rate has a peak at $\hat{s}\simeq 0.4$. Comparing the growth rates at the same absolute value $|\hat{s}|$, the negative shear $\hat{s}<0$ gives smaller growth rates than the positive shear $\hat{s}>0$ within the range $|\hat{s}|<1.7$, which is the same tendency as found in other works.[18,19] However, the critical values of $\hat{s}$, which give $\gamma=0$, have almost the same absolute value $|\hat{s}|\sim 1.7$. We should note that validity of the ballooning representation is lost in the limit $\hat{s}\to 0$ although the growth rate and real frequency for $\hat{s}=0$ is plotted in Fig. 5(a). The eigenfunctions $\phi(\theta)$ for $\hat{s}=\pm 0.8$ are shown in Fig. 5(b) where the other parameters are the same as in Fig. 5(a). We see that the imaginary parts of the eigenfunctions for the positive and negative shear cases have different signs, which implies that the phases of these eigenfunctions change differently along the field line.

Up to this point, we have examined only the cases with $\theta_k=0$, in which the mode structures are symmetric in θ and are localized around the outermost in the torus. However, in order to treat the ballooning-type mode structures in rotating toroidal systems,[23–26] it is important to take into account effects of $\theta_k\neq 0$. Figure 6(a) shows the normalized growth rate γ/ω_{*e} and real frequency ω_r/ω_{*e} as a function of θ_k for $\tau_e=1$, $\epsilon_n=0.2$, $\eta_i=2$, $\hat{s}=1$, $k_\theta\rho_s=0.75$, and $q=2$. In this case, the toroidal ITG mode is stabilized for $\theta_k>\pi/2$ where the growth rate is slightly negative and the real frequency changes little. Results for negative θ_k are not shown in Fig. 6(a) since the growth rate and real frequency are even functions of θ_k. The eigenfunctions $\phi(\theta)$ for $\theta_k=0$, 0.45π are shown in Fig. 6(b) where other parameters are the same as in Fig. 6(a). The symmetry property of the eigenfunction for $\theta_k=0$ is broken for $\theta_k=0.45\pi$. Since a significant part of the eigenfunction for $\theta_k=0.45\pi$ is contained in the good curvature region $\theta>\pi/2$ ($\theta-\theta_k>0.05\pi$), the growth rate for $\theta_k=0.45\pi$ is much reduced from that for $\theta_k=0$. It is observed that, as θ_k increases, the eigenfunction changes its shape continuously from the symmetric function of θ for $\theta_k=0$ to the antisymmetric function of $\theta-\pi$ for $\theta_k=\pi$. The growth

rate for a slowly rotating system is given by the θ_k-average $(2\pi)^{-1}\oint d\theta_k\ \gamma(\theta_k)$.[23–25] For the case in Fig. 6(b), the θ_k-averaged growth rate is about 40% of the growth rate for $\theta_k=0$.

V. CONCLUSIONS

In this work, the temporal evolution of the toroidal ITG mode has been studied by examining its damping behavior specifically. The kinetic integral equation including the initial condition is derived from Laplace transforms of the ion gyrokinetic equation, the electron Boltzmann relation, and the quasineutrality condition, in order to investigate the initial value problem. We have shown how to evaluate analytic continuation of the integral kernel as a function of a complex-valued frequency, which is useful in calculating asymptotic damping behavior of perturbations analytically and numerically.

We have found that, in the presence of the toroidal ∇B-curvature drift, the temporal dependence of the density and potential perturbations consists of normal modes and a continuum mode. The normal modes show exponential time dependence, with frequencies and growth rates determined by the dispersion relation, and they correspond to poles of the Laplace-transformed potential function in the complex frequency plane. The continuum mode is given by the integration of the Laplace-transformed potential function along a branch cut, which appears due to the toroidal ∇B-curvature drift. The long-time asymptotic behavior of the continuum mode is characterized by the power law decay $\propto t^{-2}$, which is the same as that of the ballistic response obtained with the propagator of the gyrokinetic equation without taking account of interaction with the potential. In the case where the system is unstable, the normal mode with the largest growth dominantly describes the long-time behavior. However, in the stable case where all normal modes have negative growth rates, the continuum mode survives a longer time than the normal modes. Since the power-law decay appears only when the stable normal modes are well damped,[11] then the amplitude of the continuum mode may be too small to affect the saturation level of the unstable modes for the nonlinear case. Also, finite collisional effects, if included, may easily prevent the appearance of the power-law decay. Thus, the turbulence saturation, which requires the linearly stable modes as an energy sink, is not considered to depend on the continuum mode so much as on the normal modes, although the nonlinear analysis is necessary for more detailed study.

The efficacy of the analytical continuation method shown in this work is shown by numerically obtaining the dependencies of the normal modes' growth rate, real frequency, and eigenfunction on the ion-temperature-gradient parameter η_i, the poloidal wave number k_θ, the magnetic shear parameter $\hat{s}$, and the ballooning angle parameter θ_k for both stable and unstable cases. The reductions of the growth rate due to the negative magnetic shear and due to the nonzero θ_k are confirmed, which are consistent with the internal transport barrier (ITB) formation observed in the large tokamaks with the negative magnetic shear and sheared rotation.[20–22] However, more elaborate investigation of the ITB formation is done by considering simultaneously several other effects, which are not included in this work, such as negative shear stabilization of the trapped-electron mode and stabilization of the ITG mode due to the Shafranov shift resulting from the increase of the safety factor in the core region for the negative shear case.[26]

ACKNOWLEDGMENTS

Part of this work was completed during the author's visit to the Princeton Plasma Physics Laboratory as an exchange researcher of the Joint Institute for Fusion Theory, US–Japan Fusion Cooperation Program. The author thanks Dr. G. Rewoldt for his useful comments on the work. He also appreciates discussions with Drs. G. W. Hammett and M. A. Beer. This work is partially supported by a Grant-in-Aid from the Japanese Ministry of Education, Science and Culture.

[1] W. Horton, in *Ion Temperature Gradient Driven Turbulent Transport*, edited by W. Horton, M. Wakatani, and A. J. Wooton (American Institute of Physics, New York, 1994), p. 3.
[2] J. Q. Dong, W. Horton, and J. Y. Kim, Phys. Fluids B **4**, 1867 (1992).
[3] F. Romanelli, Phys. Fluids B **1**, 1018 (1989).
[4] C. Z. Cheng and K. T. Tsang, Nucl. Fusion **21**, 643 (1981).
[5] G. Rewoldt and W. M. Tang, Phys. Fluids B **2**, 318 (1990).
[6] M. Kotschenreuther, G. Rewoldt, and W. M. Tang, Comput. Phys. Commun. **88**, 128 (1995).
[7] G. W. Hammett, M. A. Beer, W. Dorland, S. C. Cowley, and S. A. Smith, Plasma Phys. Controlled Fusion **35**, 973 (1993).
[8] D. R. Nicholson, *Introduction to Plasma Theory* (Wiley, New York, 1983), p. 76.
[9] P. Similon, J. E. Sedlak, D. Stotler, H. L. Berk, W. Horton, and D. Choi, J. Comput. Phys. **54**, 260 (1984).
[10] J. Y. Kim, Y. Kishimoto, W. Horton, and T. Tajima, Phys. Plasmas **1**, 927 (1994).
[11] T. Kuroda, H. Sugama, R. Kanno, M. Okamoto, and W. Horton, J. Phys. Soc. Jpn. **67**, 3787 (1998).
[12] P. H. Rutherford and E. A. Frieman, Phys. Fluids **11**, 569 (1968).
[13] J. B. Taylor and R. J. Hastie, Plasma Phys. **10**, 479 (1968).
[14] R. D. Hazeltine and J. D. Meiss, *Plasma Confinement* (Addison-Wesley, Redwood City, CA, 1992), p. 298.
[15] R. L. Dewar and A. H. Glasser, Phys. Fluids **26**, 3038 (1983).
[16] R. Courant and D. Hilbert, *Methods of Mathematical Physics*, Vol. 1 (Interscience, New York, 1953), Chap. 3.
[17] M. A. Beer and G. W. Hammett, Phys. Plasmas **3**, 4046 (1996).
[18] J. Y. Kim and M. Wakatani, Phys. Plasmas **2**, 1012 (1995).
[19] J. Q. Dong, Y. Z. Zhang, S. M. Mahajan, and P. N. Guzdar, Phys. Plasmas **3**, 3065 (1996).
[20] F. M. Levinton, M. C. Zarnstorff, S. H. Batha, M. Bell, R. E. Bell, R. V. Budny, C. Bush, Z. Chang, E. Fredrickson, A. Janos, J. Manickam, A. Ramsey, S. A. Sabbagh, G. L. Shmidt, E. J. Synakowski, and G. Taylor, Phys. Rev. Lett. **75**, 4417 (1995).
[21] E. J. Strait, L. L. Lao, M. E. Mauel, B. W. Rice, T. S. Taylor, K. H. Burrell, M. S. Chu, E. A. Lazarus, T. H. Osborne, S. J. Thompson, and A. D. Turnbull, Phys. Rev. Lett. **75**, 4421 (1995).
[22] T. Fujita, S. Ide, H. Shirai, M. Kikuchi, O. Naito, Y. Koide, S. Takeji, H. Kubo, and S. Ishida, Phys. Rev. Lett. **78**, 2377 (1997).
[23] W. A. Cooper, Plasma Phys. Controlled Fusion **30**, 1805 (1988).
[24] J. B. Taylor and H. R. Wilson, Plasma Phys. Controlled Fusion **38**, 1999 (1996).
[25] H. Sugama and W. Horton, in *Two-dimensional Turbulence in Plasmas and Fluids*, edited by R. L. Dewar and R. W. Griffiths (American Institute of Physics, New York, 1997), p. 275.
[26] G. Rewoldt, L. L. Lao, and W. M. Tang, Phys. Plasmas **4**, 3293 (1997).